MODELLING APPROACH TO THE MICROSTRUCTURE EVOLUTION IN COMMERCIALLY PURE ALUMINIUM DURING THE RFW PROCESS

E. HEPPNER* and E. WOSCHKE**

*Institute of Mechanics, Otto-von-Guericke University of Magdeburg, 39106 Magdeburg, Germany, eric.heppner@ovgu.de
**Institute of Mechanics, Otto-von-Guericke University of Magdeburg, 39106 Magdeburg, Germany, elmar.woschke@ovgu.de

DOI 10.3217/978-3-85125-615-4-35

ABSTRACT

The rotary friction welding (RFW) is nowadays a well-established joining technique since it is highly productive, entirely repeatable, and very economical. It belongs to the solid-state fusing methods allowing the combination of similar and for a wide spectrum of dissimilar materials. Commonly combined are aluminium and steel materials to manufacture high quality lightweight structures with excellent technological properties. Due to the fact that the welding temperature does not exceed the material's melt temperature, microstructural transformations only appear caused by the heating and cooling rate and the amount of plastic deformation. Aluminium alloys in particular show a pronounced change in microstructure as a consequence of dynamic recrystallization evoked by the high degree of plastic deformation. The purposes of this paper is to present a modelling approach to the microstructure evolution in commercially pure aluminium, for aluminium to steel friction welded joints. The main motivation therein is the consistent prediction of the recrystallization rate of different layers in the process affected zone for an improved understanding of microstructural evolution during the RFW process.

Keywords: rotary friction welding, aluminium, steel, dissimilar materials, microstructure modelling, welding simulation

INTRODUCTION

Present-day research in the flied of product development are increasingly focused on the efficient use of energy and raw material resources. In the light of this, the design principle of consistent lightweight construction is gaining more and more importance. One possible approach is the targeted exploitation of technological properties of different materials in hybrid structures. The objective is always to continuously improve the product properties in terms of functional performance, safety and frequency, as well as to reduce the use of resources and energy consumption. Depending on their field of application, in the automotive and transport industry, tool and fixture construction and in the aerospace

industry, hybrid structures often consist of combinations of metallic materials with aluminium alloys.

Against this background, a considerable number of established joining methods can only be used to a limited extent. Either they do not take into account the differences in material's behaviour in the manufacturing process (e.g. different melting temperatures referring to fusion welding) or they greatly increase the effort for the joining operation by adding additional joining elements (e.g. by riveting or screwing). Due to this face, joining techniques based on plastic deformation, like the rotary friction welding (RFW), are particularly advantageous. It allows the joining of similar and dissimilar materials without passing the material's melt temperature and without using any filler material or inert gas. Further benefits are the short manufacturing cycling time, the high joint quality and the good automatization potential.

In the RFW, commonly rotationally symmetrical workpieces are welded by using the frictional heat and the axial pressure. Fig. 1 illustrates the general setup wherein one part (A) is static and the other part (B) is rotating and pressed on producing the frictional heat in the contact area. The determining process parameters thereby are the axial force (F), the axial shift (s) and the rotary speed (n).

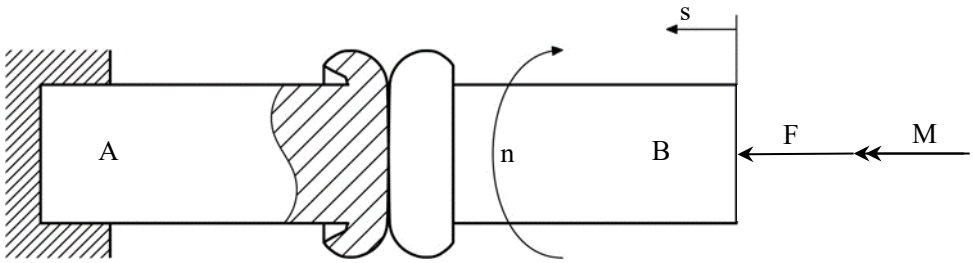

Fig. 1 General structure of the rotary friction welding process [1]

The usual procedure consists of two fundamental process stages being the rubbing (I) and the forging stage (II) whose characteristics are strongly link to the type of machine drive (directly or fly wheel driven). The decisive difference between these two variants is related to the rotation speed curve of the spindle (Fig. 2). In fly wheel friction welding, the rotary speed is applied and decelerated in a self-regulated manner depending on storaged energy by the inertia of the fly wheel. By contrast, in the direct driven friction welding process it is done by a continuously driven engine. Hence, these variants are known as inertia friction welding (IFW) and direct driven friction welding (DDFW).

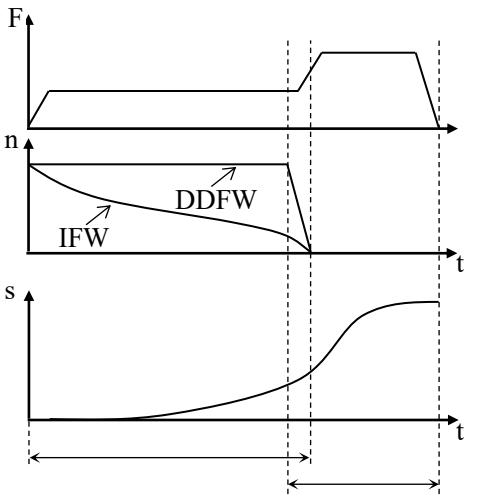

Fig. 2 Parameter regime of the IFW process in contrast to the DDFW process [1]

Concerning interfacial material bond, it can be stated that its creation is based on solid-state reactions in the contact area between the different former separated substance systems of the involved welding materials. The required activation energy thereby is provided by the frictional heat and supported by the elastoplastic deformation of the underlying material. In order to enable the substance systems interaction it is necessary to replace all contaminants and oxide layers out of the interface. This is accomplish during the material's deformation the rubbing and forging stages while they are first cracked and afterwards spread out into the resulting flash. With respect to the interdiffusion process it has to be emphasized that its occurrence is an attendant phenomenon of the material bonding during the welding procedure leading to new intermediate material layers. These layers are the result of the changes of the chemical composition in the contact area and mainly consist of intermetallic compounds.

Due to the fact that the welding temperature does not exceed the material's melt temperature, micro-structural transformations only appear caused by the heating and cooling rate and the degree of severe plastic deformation. With this in mind, aluminium to steel friction welded joints were analysed with respect to their microstructure after the welding procedure. Several studies [2–4] indicated that only the aluminium material undergoes a pronounced change in microstructure due to the fact of lack any deformation on the steel side. According to the location on the aluminium side an increase of the dynamic recrystallization volume from the unaffected base material to the contact area was recognized.

Against this background, this paper is presenting an ansatz to simulate the dynamic recrystallization in commercially pure aluminium during the RFW process based on an Avrami-typ equation. Further scenarios, such as precipitation and strain hardening or coarsening, are purposely not modelled. On the one hand, these microstructural transformations do not occur in commercially aluminium (precipitation hardening) and on the other hand, they do not taken place during the RFW process (strain hardening and coarsening).

Since, the passed welding temperatures and degree of plastic deformation are required, it is essential to map the thermal and deformation cycles itself through a RFW process

simulation. Nevertheless, the process simulation is completely independent from the microstructure simulation and serves exclusively to determine the state variables (temperature and degree of deformation history) for the Avrami equation.

The outline of this paper is as following: First of all, the derivation of the microstructure evolution equation and its computational treatment is shown in common with an introduction to the RFW process modelling ansatz. Later, the simulation results are displayed corresponding with their related experimental data analysis. Finally, the results are summarized up and an outlook for the further actions is given.

THEORETICAL BACKGROUND AND METHODOLOGY

MICROSTRUCTURE MODELLING

Starting point for basically description of phase transition or structural transformation phenomena in solids under isothermal and unstressed conditions is the general Johnson-Mehl-Avrami-Kolmogorow equation, commonly known as Avrami equation. Hence, it is used to model the static recrystallization in aluminium alloys shown by [5]

$$\chi = 1 - \exp\left(-\alpha t^{\beta}\right). \tag{1}$$

Therein are χ the recrystallization volume fraction, α the overall rate constant and β the Avrami exponent. Generally α and β are temperature dependent and have to be experimentally estimated. Due to the conditional limitations [6] consistently modified this evolution equation to describe also the dynamic recrystallization by taking the part of the plastic strain ε instead of the time

$$\chi = 1 - \exp\left(-\alpha \varepsilon^{\beta}\right). \tag{2}$$

Various investigations [7,8] confirmed its validity for different aluminium alloys whereas it has to stated that this approach is only phenomenologically justified and needs to be reviewed for the considered case. With this in mind, the correctness will be discussed later. In this paper a further modification is made with the purpose to consider also non-isothermal and non-steady-state conditions. For that reason, Eqn. (2) was derived in time and subsequently the plastic strain was eliminated by employing the recrystallization volume fraction

$$\dot{\chi} = \alpha\beta(1-\chi)\left(\frac{-\ln(1-\chi)}{\alpha}\right)^{\frac{\beta-1}{\beta}} \dot{\varepsilon}. \tag{3}$$

The resulting differential equation is no more limited to isothermal and steady-state conditions. Its computational integration can be done by the Runge-Kutta procedure, for instance. Here, the applied strain rate $\dot{\varepsilon}$ is related to a 1D problem, hence it can easily be estimated by the direct time derivation of the plastic strain. In case of 3D problems like the

FRW process, the von-Mises equation can be used under the assumption of volume constancy. Therefore, the symmetric part of deformation rate gradient tensor **D** is adopted

$$\dot{\varepsilon} = \sqrt{\frac{2}{3}\mathbf{D}\cdot\mathbf{D}} \tag{4}$$

as well as the deformation gradient tensor **F**

$$\mathbf{D} = \frac{1}{2}\left(\dot{\mathbf{F}} \cdot \mathbf{F}^{-1} + \mathbf{F}^{-T} \cdot \dot{\mathbf{F}}^{T}\right). \tag{5}$$

THERMAL AND DEFORMATION CYCLE MODELLING

First attempts of modelling the RWF process can be dated back to the mid 1990's by [9] and followed later by [10–13] always with the purpose of developing a robust simulation tool to be capable to understand and improve the welding process. Nowadays, a new modelling approach from [14] gain more and more attention caused by its computational time efficiency, high robustness and stability. In view of these benefits, this modelling approach is also used here. In the following a few comments to the general procedure and to the main governing equations are given. Due to the fact, that the RFW process is a deformation with temperature coupled problem, two essential differential equations have to be solve. One is related to the description of the motion of continua. At this point, it is represented in its weak form by the principle of virtual power

$$\int_{\mathcal{B}} \delta\mathbf{v} \cdot \ddot{\mathbf{x}}\, \rho \mathrm{dV} = \int_{\mathcal{B}} \delta\mathbf{v} \cdot \mathbf{b}\, \rho \mathrm{dV} + \int_{\mathcal{B}} \delta\mathbf{v} \cdot \mathrm{div}(\boldsymbol{\sigma})\, \mathrm{dV}. \tag{6}$$

Here, the acceleration is depicted by $\ddot{\mathbf{x}}$, **b** is related to the inner body forces, $\boldsymbol{\sigma}$ is the Cauchy stress tensor and ρ describes the mass density. The other equation concerns to the heat conduction in the welding components and is mapped in its weak form by the principle of virtual temperature

$$\int_{\mathcal{B}} \delta\Theta c\dot{\Theta}\rho\, \mathrm{dV} = \int_{\mathcal{B}} \delta\Theta r\rho\, \mathrm{dV} - \int_{\mathcal{B}} \delta\Theta\, \mathrm{div}(\mathbf{q})\, \mathrm{dV} + \int_{\mathcal{B}} \delta\Theta\, \boldsymbol{\sigma} \cdot\cdot\, \mathbf{D}\, \mathrm{dV}. \tag{7}$$

Incidentally, Θ expresses the absolute temperature, $\boldsymbol{\sigma} \cdot\cdot\, \mathbf{D}$ is the dissipation energy of the inner stresses, **q** represents the heat flux and r is the mass specific heat source term. Both initial value problems are solved by the help of the finite element method and the use of a penalty contact formulation. Further details concerning the modelling of the friction or the environmental modelling can be seen in [14].

Another issue in the RFW modelling affects the material deformation behaviour. The most challenging part therein is to cover the large elastoplastic deformation over the entire welding temperature range with simultaneous consideration of the immense changes in the rate of deformation. The main innovation in [14] is the use of an advanced Carreau fluid model to describe the material behaviour during the process. As a consequence, the Cauchy

stress is just a function of the current deformation rate gradient tensor, the temperature and the von-Mises strain rate

$$\boldsymbol{\sigma} = \mu_{\mathrm{B}}\,\mathrm{tr}(\mathbf{D})\,\mathbf{I} + 2\mu(\dot{\varepsilon}, \Theta)\mathrm{dev}(\mathbf{D}). \tag{8}$$

The advantages of this formulation in contrast to others are its improved approximation of the stress-strain rate relation in the higher temperature ranges and the better tangibility of the material parameters. The employed shear viscosity $\mu(\Theta, \dot{\varepsilon})$ is derived form a Norton-Bailey power law

$$\mu(\dot{\varepsilon}, \Theta) = \left[1 + \left(\left(\frac{\sigma_0(\Theta)}{3\mu_0\dot{\varepsilon}_0}\right)^{\frac{n}{1-n}}\frac{\dot{\varepsilon}}{\dot{\varepsilon}_0}\right)^2\right]^{\frac{1-n}{2n}}(\mu_0 - \mu_\infty) + \mu_\infty. \tag{9}$$

Wherein, the temperature-dependant exponent $n(\Theta)$ is consistently assessed by the assumption that all isothermal viscosity-strain rate curves finally intersect in the same point. Fig. 3 illustrates the regime of isothermal viscosity-strain rate curves for this Carreau fluid formulation.

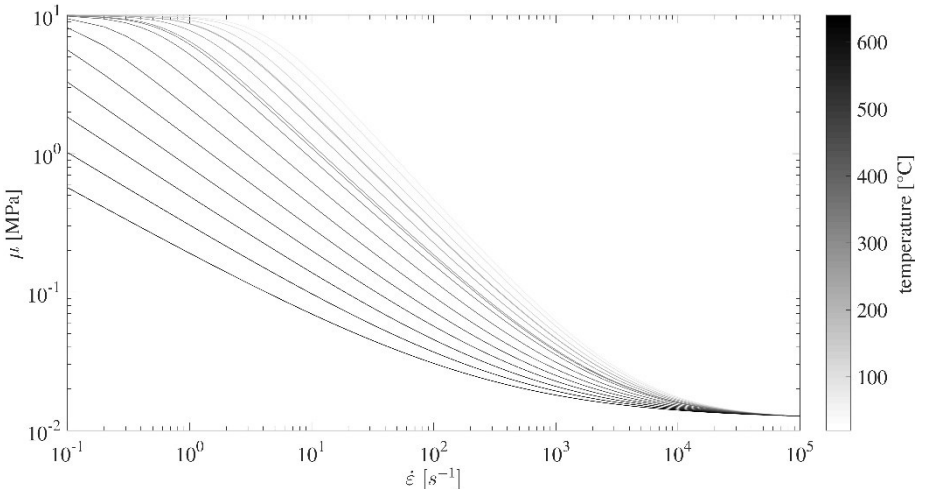

Fig. 3 Regime of isothermal viscosity-strain rate curves

The introduced saturation parameters μ_0 and μ_∞ in Eqn. (9) are applied for a better computational tangibility of various singularities arising in cases of $\dot{\varepsilon} \to 0$, $\dot{\varepsilon} \to \infty$ and $\Theta \geq \Theta_{\mathrm{M}}$. Whereas, the adopted bulk viscosity linked to the spherical part of the Cauchy stress tensor in Eqn. (8) is in order to preserve the volume constancy and acts in this way like a Lagrange multiplier. The reference strain rate $\dot{\varepsilon}_0$ and the reference flow stress $\sigma_0(\Theta)$ in Eqn. (8) arisen from Norton-Bailey power law are material specific constants. Additional detailed information regarding the local and temporal discretization, the finite element formulation and the meshing respectively the remeshing procedure, can be found in [14].

EXPERIMENTAL AND SIMULATION RESULTS

This section is demonstrating the potential and the performance of the aforementioned simulation methodology for the microstructural evolution in commercially pure aluminium during the RFW process. The focus lies on the qualitative prediction of the dynamic recrystallized volume fraction according to the location from the contact area to the unaffected base material. For that purpose, a commercially pure aluminium (EN AW-1050A) to structural steel (S355JR) direct driven friction welded joint was analysed. The used process parameterization set is displayed in Table 1.

Table 1 Process parameterization

friction pressure [MPa]	forging pressure [MPa]	friction time [s]	forging time [s]	rotary speed [$\mathbf{min^{-1}}$]
20	60	1	3	7500

Since, only the aluminium underwent a relevant change in microstructure, the examination of the steel side was neglected. Fig. 4 shows the cross-section of the weld pointing out the investigation area for the microstructural analysis.

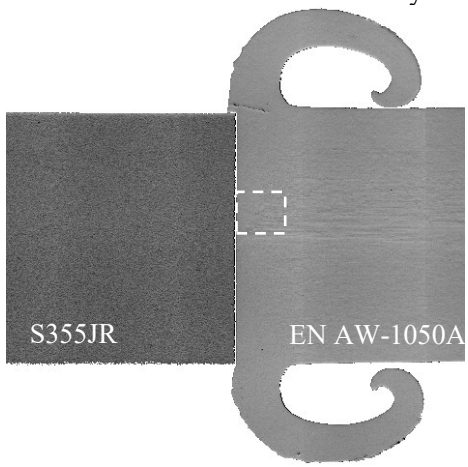

Fig. 4 Cross-section of the weld displaying the investigation area

In accordance with [15], Fig. 5 represents two different layers with microstructural transformations, commonly known as, dynamically recrystallized zone (DRX) and thermo-mechanically affected zone (TMAZ). The microstructure study offers fully recrystallized fine and equiaxed grains in the DRX immediately after the interface. Followed by partially dynamically recrystallized grains plus redirected unaffected grains in the TMAZ. The reason for that is based on the material flow from the inner to the outer body during the manufacturing process and effects in this way a turn round of the former axial-directed grains to the radial direction (exemplified by two arrows in Fig. 5). Furthermore, the analysis of the base material (BS) expectedly displays an unaffected microstructure due to the lack of thermal and plastic deformation. In agree with [15], these results are typically observed for aluminium to steel friction welded joints.

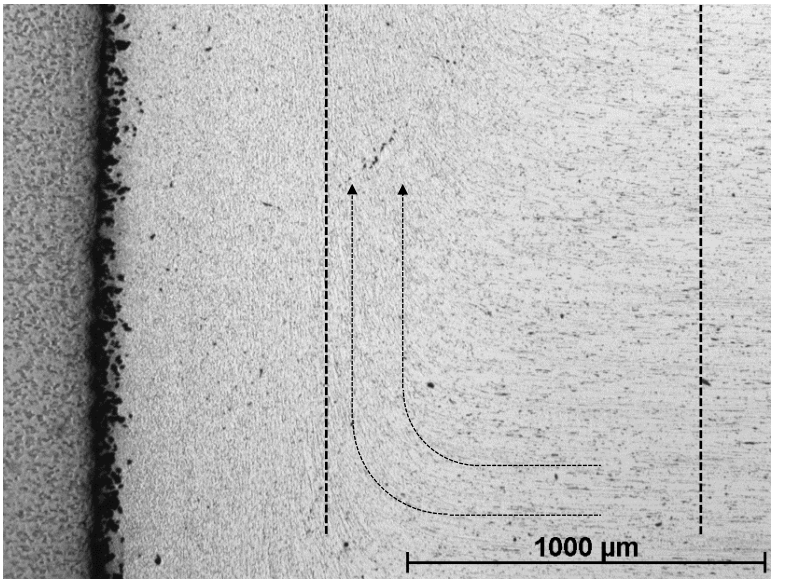

Fig. 5 Optical microstructure taken from near-centre region

Table 2 lists the measured mean grain sizes corresponding to their appearance in these zones.

Table 2 Process parameterization

DRX [µm]	TMAZ [µm]	BS [µm]
7	11-45	73

As a consequence of the microstructural study, every individual zone indicates a distinctive percentage of dynamically recrystallized volume being $\chi = 1$ for the DRX, $0 < \chi < 1$ for the TMAZ and $\chi = 0$ for the base material. Nevertheless, it has to be stated that an exact experimental estimation of the range of every single zone is quiet difficult due to the fact that the transition into each other is flowing. With this in mind, here is just a qualitatively comparison of the dynamically recrystallized volume fraction between the model and the experiment done. Fig. 6 illustrates the computational results of the microstructural evolution based on the previous described modelling method and clarifies the area of experimental investigation (Fig. 6).

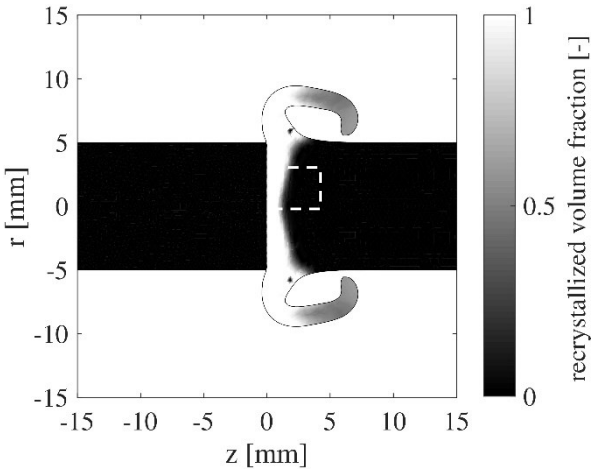

Fig. 6 Regime of the dynamically recrystallized volume fraction

All in all, it can be stated that a qualitatively good agreement with the experimental investigation is achieved. The simulation maps the regime of microstructural transformation from the unaffected base material to the DRX quiet well. However, the expanse of TMAZ is only insufficient mapped and indicates a very narrow transition between the DRX and the BS unlike it was observed by the microscopic analysis (Fig. 5). One reason for this concerns the lack of knowledge of the exact material specific parameters α and β for the related von-Mises strain rates and temperatures. Here, these data have been estimated using the method described in [8] with the help of the tensile test data from [16]. Another reason is related to the exact computation of the required temperatures and the von-Mises strain rates, commonly known as state variables, mapped by the process simulation for the entire welding procedure. Fig. 7 and Fig. 8 display exemplary the temperature and the von-Mises strain rate immediately after the rubbing stage at t = 1.5 s.

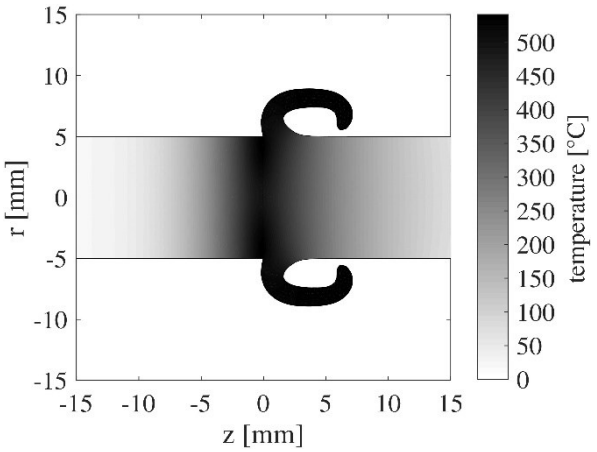

Fig. 7 Temperature immediately after the rubbing stage at $t = 1.5\ s$

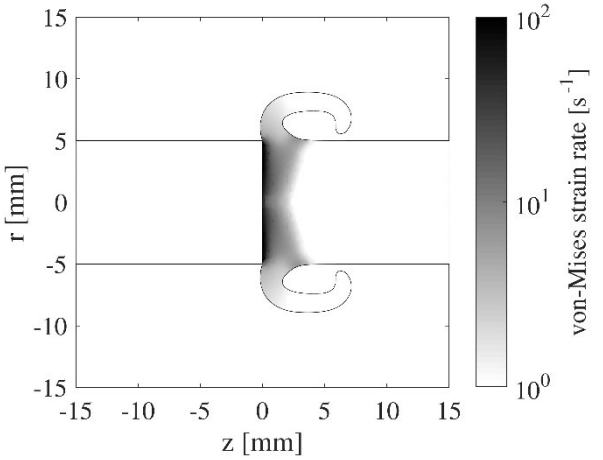

Fig. 8 von Mises strain rate immediately after the rubbing stage at $t = 1.5\ s$

Basically, there are almost no satisfying possibilities to determine these state variables during the process experimentally. Therefore, no direct comparison between the process simulation results and reality can be made. For this reason, other options must be used to validate the simulation. [14] pointed out that the agreement of the flash evolution between the simulation and the experiment is an excellent indicator for the simulation quality and thus also for validity of the corresponding state variables. Fig. 9 illustrates the comparison of the flash evolution between the model and experiment for the analysed joint.

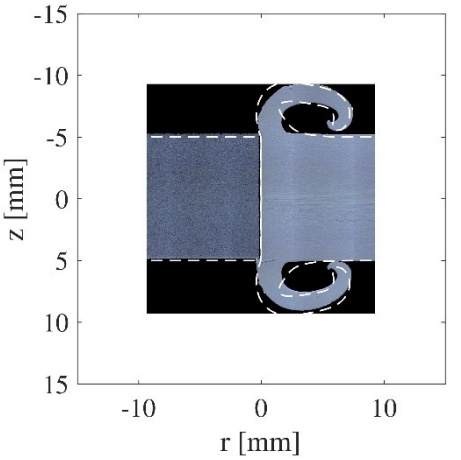

Fig. 9 Comparison of the simulated and the experimental obtained flash at the end of the forging stage

Despite some small deviations in the flash evolution, it can be assumed that the mapping of the process and the related state variables is not the cause for the differences in the microstructure simulation. Rather, it has to be worked on a better estimation of the material specific parameter for the modified Avrami equation to achieve an even better approximation.

CONCLUSION

In the current paper, a modelling ansatz for the microstructural evolution in commercially pure aluminium was represented. The main purpose therein was the simulation of the dynamic recrystallization due to its dominating rule during the RFW process. Therefore, the generally Avrami equation was modified in order to consider dynamic recrystallization for non-isothermal and non-steady-state conditions. The obtained results indicate a qualitatively good agreement with the experimental investigation. Benefits of this model are the proper estimation of the dynamic recrystallized volume fraction and by the means of a mixing rule the determination of the resulting grain size.

REFERENCES

[1] D. SCHMICKER, K. NAUMENKO, AND J. STRACKELJAN, "A robust simulation of Direct Drive Friction Welding with a modified Carreau fluid constitutive model," *Computer Methods in Applied Mechanics and Engineering*, vol. 265, pp. 186–194, 2013.

[2] M. SAHIN AND C. MISIRLI, "Mechanical and Metalurgical Properties of Friction Welded Aluminium Joints," in *Pure 7000 Alloys: Microstructure, Heat Treatments and Hot Working,* P. Leo and E. Cerri, Eds., INTECH Open Access Publisher, 2012.

[3] M. YILMAZ, M. ÇÖL, AND M. ACET, "Interface properties of aluminum/steel friction-welded components," *Materials Characterization*, vol. 49, no. 5, pp. 421–429, 2002.

[4] M. ASHFAQ, N. SAJJA, H. KHALID RAFI et al., "Improving Strength of Stainless Steel/Aluminum Alloy Friction Welds by Modifying Faying Surface Design," *Journal of Materials Engineering and Performance*, vol. 22, no. 2, pp. 376–383, 2013.

[5] M. AVRAMI, "Kinetics of Phase Change. I. General Theory" *Journal of Chemical Physics*, vol. 7, no. 12, pp. 1103–1112, 1939.

[6] Q. GUO-ZHENG, "Characterization for Dynamic Recrystallization Kinetics Based on Stress-Strain Curves," in *Recrystallization Processes Involving Iron Oxides in Natural Environments and In Vitro,* N. Taitel-Goldman, Ed., INTECH Open Access Publisher, 2013.

[7] K. HUANG AND R. E. LOGÉ, "A review of dynamic recrystallization phenomena in metallic materials," *Materials & Design*, vol. 111, pp. 548–574, 2016.

[8] Y.-B. HE, Q.-L. PAN, Q. CHEN et al., "Modeling of strain hardening and dynamic recrystallization of ZK60 magnesium alloy during hot deformation," *Transactions of Nonferrous Metals Society of China*, vol. 22, no. 2, pp. 246–254, 2012.

[9] V. K. STOKES AND A. J. POSLINSKI, "Effects of variable viscosity on the steady melting of thermoplastics during spin welding," *Polymer Engineering and Science*, vol. 35, no. 5, pp. 441–459, 1995.

[10] L. D'ALVISE, E. MASSONI, AND S. J. WALLØE, "Finite element modelling of the inertia friction welding process between dissimilar materials," *Journal of Materials Processing Technology*, 125-126, pp. 387–391, 2002.

[11] A. MOAL AND E. MASSONI, "Finite element simulation of the inertia welding of two similar parts," *Engineering Computations*, vol. 12, no. 6, pp. 497–512, 1995.

[12] G. J. BENDZSAK, T. H. NORTH, AND Z. LI, "Numerical model for steady-state flow in friction welding," *Acta Materialia*, vol. 45, no. 4, pp. 1735–1745, 1997.

[13] L. WANG, M. PREUSS, P. J. WITHERS et al., "Energy-input-based finite-element process modeling of inertia welding," *Metallurgical and Materials Transactions B*, vol. 36, no. 4, pp. 513–523, 2005.

[14] D. SCHMICKER, *A holistic approach on the simulation of rotary friction welding,* Dissertation, Fakultät für Maschinenbau; epubli GmbH, 2015.

[15] M. ASHFAQ AND K. J. RAO, "Comparing bond formation mechanism between similar and dissimilar aluminium alloy friction welds," *Materials Science and Technology*, vol. 30, no. 3, pp. 329–338, 2014.

[16] E. DOEGE, H. MEYER-NOLKEMPER, AND I. SAEED, *Fließkurvenatlas metallischer Werkstoffe*: *Mit Fließkurven für 73 Werkstoffe und einer grundlegenden Einführung*, Hanser, München, 1986.